Contents lists available at ScienceDirect

Chemical Engineering Journal

Experimental investigation of single particle settling in turbulence generated by oscillating grid

Qi Zhou, Nian-Sheng Cheng*

School of Civil and Environmental Engineering, Nanyang Technological University, Nanyang Avenue, Singapore 639798, Singapore

ARTICLE INFO

ABSTRACT

In this study, turbulence influence on the settling behavior of solid particles was investigated experimentally in confined turbulent aquatic environment generated by oscillating grid. An enhanced PIV system was employed to conduct simultaneous velocity measurements of individual settling particles and ambient fluid. Grains varying in shape (spherical and cylindrical) and diameter (2.78–7.94 mm) were tested with different turbulent conditions.

The results showed clearly that the settling behavior of particles subjected to turbulence is significantly modified. First, the settling velocity modification is closely correlated to the mean vertical velocity of the fluid zone (very close to the settling particle), which in size is in the order of a few particle diameters. Second, the relative settling velocity is smaller than the still water terminal velocity for the most cases. Lastly, the fluctuation in the settling velocity is significantly increased, as compared to the still water conditions, and clearly dependent on the turbulence intensity.

The experimental data were also analyzed with dimensional considerations. By comparing to literature, turbulence effects on the relative settling velocity were discussed with regard to Stokes number, Richardson number and dimensionless turbulence length scale. Finally, a simple analytical model was proposed for estimating the turbulence-modified settling velocity.

© 2008 Elsevier B.V. All rights reserved.

1. Introduction

Knowledge of the behavior of solid particles settling through fluids is of fundamental importance for numerous industrial and environmental multiphase-flow applications involving particle suspension and transport. However, existing empirical and semi-empirical expressions for the computation of particle settling velocity are limited to the case where fluid phase is quiescent, while in most applications the carrier fluid is in motion and usually turbulent.

Experimental studies addressing turbulence effects have been done for various scenarios, for example, particle-laden flows in chemical reaction vessels [1,2], sedimentation of phytoplankton cells in the surface mixing layers of natural water [3], and sediment transportation and deposition in an open channel flow [4,5]. These studies have shown that the settling velocity could be modified in the presence of turbulence, but it remains inconclusive whether settling is enhanced or retarded and how significant the modification could be, as summarized in Table 1. Magelli et al. [1] and Brucato et al. [2] reported reduction in the settling velocity of

solid particles in a stirred medium, W_s, with respect to the terminal velocity in a quiescent liquid, W_T. In these studies, the velocity ratio, W_s/W_T, was correlated with the length ratio, d/λ, where d denotes the particle diameter and λ the Kolmogorov scale of dissipative eddies. On the contrary, the phenomenon of settling velocity enhancement due to turbulence is also reported [3,6–8]. Flume tests conducted recently by Cuthbertson and Ervine [4] and Kawanisi and Shiozaki [5] showed that both modifications are possible, depending on flow configuration and turbulence intensity. Cuthbertson and Ervine [4] suggested that the inertial and lift forces were negligible as compared to the dominant gravitational and drag forces on the settling particle, and thus the relative velocity between the particle and fluid was equal to the still-water terminal velocity. A most recent study by Doroodchi et al. [9] was conducted with turbulent flows generated by a pair of grids oscillating horizontally in a water tank, showing a reduction of settling velocity up to 25% of the terminal value. Similar turbulence-generating apparatus was also employed by Zhou and Cheng [10], who however reported general enhancement of settling velocity. It should be noted that in the confined flow systems, the presence of secondary flows is not avoidable in spite of optimized grid configurations [3,10]. Though generally weak, the secondary flows may affect the settling velocity to a certain degree. Unfortunately, such effects have not been examined in the abovementioned studies because

* Corresponding author. Tel.: +65 6790 6936; fax: +65 6791 0676.
E-mail address: cnscheng@ntu.edu.sg (N.-S. Cheng).

Nomenclature

C	constant
C_A	added mass coefficient
C_D	drag coefficient
C_{D0}	standard drag coefficient
d	particle diameter
d_*	volume-equivalent nominal particle diameter
f	grid oscillating frequency
g	gravitational acceleration
k	turbulent energy
L	integral length scale
M	mesh size
n_1	number of the velocity vectors for each PIV image pair
n_2	number of PIV image pairs for each run
N	averaging window size for each run
Re	Reynolds number
Re_p	particle Reynolds number in still water
S	stroke
St	Stokes number
t_p	Stokes response time
u	instantaneous horizontal flow velocity
v	instantaneous vertical flow velocity
U	mean horizontal flow velocity
V	mean vertical flow velocity
U'	RMS horizontal velocity fluctuation
V'	RMS vertical velocity fluctuation
W_s	settling velocity in turbulent water
W_s'	settling velocity fluctuation
W_T	terminal velocity in still water
z	vertical distance from grid mid-plane

Greek letters

ε	turbulent energy dissipation rate
λ	Kolmogorov length scale of dissipative eddies
ν	kinematic viscosity
ρ	fluid medium density
ρ_s	solid particle density
τ_p	particle relaxation time

of difficulties encountered in simultaneous two-phase measurements.

Various quantities, including particle characteristics (size, density) and turbulence characteristics in terms of length, time or velocity scales, have been considered in previous studies. Particle–turbulence interaction can be characterized by various derived quantities such as length, time and velocity scales. One of widely used parameters is the Stokes number St, which is defined as the ratio of particle characteristic time scale to the Kolmogorov time scale of turbulence. This parameter is often employed to describe the ability of a particle to follow the fluid motions, or the "sensitivity" of the particle to the turbulence disturbance. Friedman and Katz [8] showed that the rising rate of fuel droplet in water is strongly dependent on St at intermediate turbulence intensity. Yang and Shy [11] studied the settling behavior of heavy particles in an aqueous near-isotropic turbulence generated by a pair of oscillating grids. They presented that the magnitude of settling velocity enhancement reaches its maximum as St is nearly unity, which is consistent with the numerical results given by Wang and Maxey [12], and Yang and Lei [6]. Cuthbertson and Ervine [4] studied the particle settling in turbulent open channel flow and reported that the degree of settling enhancement would be maximized for fine particles with low shear particle Reynolds number and $St \approx 1$, while small-scale tur-

Table 1
Summary of previous experimental studies.

Researchers	Carrier fluid	Settling/rising objects			Velocity measurement techniques	Turbulence effect on settling/rising
		Material	d (mm)	ρ (g/cm^3)		
Magelli et al. [1]	Liquid flow in vessels stirred with multiple propellers	Glass beads, etc.	0.14–0.33	1.02–2.45	Computation by solid concentration profile	Retardation
Brucato et al. [2]	Liquid flow between two co-axial rotating cylinders (Couette–Taylor flow field)	Silica and glass beads	0.063–0.500	2.5	Residence time technique	Retardation
Aliseda et al. [7]	Air in horizontal wind tunnel	Water droplets	–	1.0	Hot-wire anemometry and PDPA	Enhancement
Friedman and Katz [8]	Liquid flow generated by four rotating grids	Diesel fuel droplets	0.3–1.5	0.85	PIV	Enhancement
Yang and Shy [11]	Water flow generated by a pair of vertically oscillating grids	Tungsten and glass particles	0.060–0.505	2.5 and 19.3	PIV and PTV	Enhancement
Ruiz et al. [3]	Liquid flow generated by rotating thin cylinder and oscillating grid respectively	Phytoplankton cells	–	≈1.0	Particle image processing	Enhancement
Cuthbertson and Ervine [4]	Turbulent open channel liquid flow	Natural sands	0.181–0.463	2.65	ADV and particle tracking by high speed camera	Both enhancement and retardation
Doroodchi et al. [9]	Flow field in water tank generated by a pair of horizontally oscillating grids	Teflon and Nylon particles	2.38–7.94	2.30, 1.14	High speed camera	Retardation
Present study	Turbulent water flow generated by oscillating grid	Polystyrene	2.79–7.94	1.050–1.077	PIV	Retardation for slip velocity

Notes: PDPA: phase Doppler particle analysis; PIV: particle image velocimetry; PTV: particle tracking velocimetry; ADV: acoustic Doppler velocimeter.

bulence might have little or no influence on coarser particles under the dominant gravitational effect for $St \gg 1$.

Mechanism responsible for the turbulence modification to the particle settling velocity has also been propounded by several studies with analytical and numerical attempts. On one hand, mechanism accounting for a settling velocity reduction includes non-linear drag [13] and loitering effect [14]. The former was demonstrated by a Monte Carlo simulation showing the effect of nonlinearity of the drag associated with turbulence. So-called loitering effect was analytically studied by considering a settling particle in a steady, non-uniform flow field with a specific, highly organized vortex structure. The results showed that the particle spends relatively longer time for the specified flow configuration and the settling velocity is hence reduced. On the other hand, the most frequently mentioned mechanism for settling enhancement is preferential sweeping, or trajectory biasing. It refers to the phenomenon of preferential sweeping motion on the down-flow side of local vortices due to the local centrifugal effect, which leads to enhanced settling rates. By a direct numerical simulation (DNS), Wang and Maxey [12] studied the settling velocity as well as the concentration in a random flow field for heavy particles. They showed that the settling rate was significantly enhanced and the flow region of high vorticity correlated well with the region of low particle concentration, which supported the preferential sweeping. This mechanism has been frequently employed by researchers as possible explanation of their experimental results [3,4,7,8,11]. Moreover, the role of turbulent scales, from large energetic eddy to smallest Kolmogorov scale, in modifying the particle settling was also investigated. A DNS conducted by Bagchi and Balachandar [15] showed that the free stream turbulence had no substantial and systematic effects on the time-averaged drag.

This study aimed to experimentally investigate turbulence effects on the behavior of individually settling particles. First, in order to correlate the observed modification to the settling behavior to turbulent flow field, especially the characteristics of local flow close to the settling particle, both motions of the solid phase and surrounding fluid were measured simultaneously with an enhanced Particle Image Velocimetry (PIV) technique. Second, by noting that most previous researchers have concentrated their experimental efforts on the group behavior exhibited by a large number of settling particles, with the measurement of ambient fluid flows in a bulk volume (e.g. [1,2]), we conducted all experiments in a repetitive fashion and focused on the settling behavior of each single particle.

2. Experimental setup

In this study, particle settling behavior was observed in a confined turbulent environment, which was generated by placing an oscillating grid in a water tank. Turbulent flows so generated are characterized by approximately zero-mean velocity and two-dimensional homogeneity, and thus can be considered theoretically simpler than those appearing in boundary layers and open channels. Some quantitative properties of such mechanically driven turbulence have been obtained by previous researchers. Cheng and Law [16] studied the statistical characteristics of the turbulent flow field based on PIV measurements, which confirmed that the turbulence decay follows the power law proposed by Hopfinger and Toly [17]. Cheng and Law [16] also suggested that homogeneity of the turbulence be achieved only at a distance away from the grid plane by three mesh sizes. In addition, Matsunaga et al. [18] developed an analytical solution for the oscillating-grid turbulent flow based on the k–ε model. Yan et al. [19] summarized a number of achievements obtained in the study of the oscillating grid turbulence and its applications in investigating several hydraulic problems encoun-
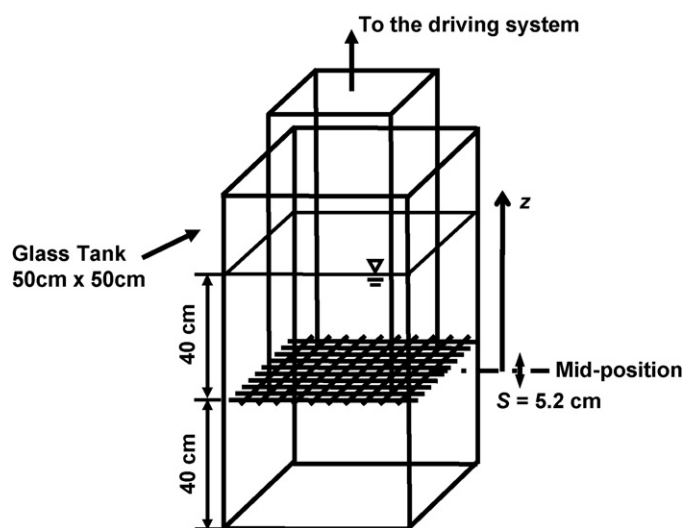

Fig. 1. Sketch of oscillating grid system.

tered in mass transfer, sediment entrainment and suspension and environmental engineering.

The flow system shown in Fig. 1 was the same as that used previously by Cheng and Law [16]. It consisted of a water glass tank, 50 cm × 50 cm in cross section and 100 cm in height, which was supported by a platform with an adjustable height, and a grid, made of square bars of 1 cm × 1 cm, with a mesh size of 5 cm and a solidity of 36%. The grid was hung vertically 40 cm above the bottom of the tank by four steel bars of 0.5 cm diameter, and then connected to a speed-controlled motor. The stroke, i.e. the amplitude of grid oscillation, was fixed to be 5.2 cm. The water level was maintained at 80 cm from the bottom of the tank.

Particles used for settling tests were washed prior to measurements and then freely released from below the water surface with great care to avoid air bubbles attached onto particle surfaces, which may affect the settling velocity. The location to release the particles was at the center of the tank to avoid possible side-wall effects. Tests were conducted at two grid oscillating frequencies, i.e. 2 Hz and 3 Hz, respectively. The settling processes for spherical particles were captured over a distance starting from $z = 3.4$ cm up to 26.3 cm, where z is the vertical distance above the mid-position of the grid. There was a distance of more than 13 cm above the imaging region for the particle to accelerate to its "terminal" velocity through turbulent water. Possible errors induced by particle acceleration are considered insignificant for this study as the data analysis of the particle motion was performed largely in the Lagrange sense. For each oscillating frequency, three 10 cm × 10 cm imaging windows, positioned at different elevations with some overlapping, were used to cover the whole vertical distance of 22.9 cm, so that particle settling behaviors were observed for vertically varied turbulent conditions.

Digital PIV technique was employed in this study to provide a planar measurement of the horizontal and vertical velocities of the background flow. In this study, the PIV system was enhanced with software platform Dantec DynamicStudio 1.30.2, which was operated with a dual-cavity Q-switched pulsed Nd:YAG laser, and a CCD camera with a resolution of 1200 × 1200 pixels. Polyamide particles with a nominal diameter of 50 μm were used as seedings to represent the fluid motion. Seeding concentration was adjusted to ensure that at least 10 particles were distributed within one interrogation area (IA). The pulse interval was carefully chosen for each test in the range of 1.0–11.5 ms depending on the flow condition, so as to ensure that the seeding particles traveled no further than one fourth of the IA dimension, and the sampling rate was set at

Table 2
Summary of grain properties.

Type	Shape	Dimensions (mm)		Density (kg/m³)	W_T (cm/s)	Re_p
I	Spherical	Diameter	6.35 7.94	1050	8.85 10.29	568 824
II	Cylindrical	Mean diameter Mean length	2.4 3.0	1077	2.05–5.92	66–198

11 Hz, which was the maximum frequency allowed by the system. The light sheet produced had a typical thickness of 0.5 mm. Images with a size of 10 cm × 10 cm were captured by CCD camera, and then analyzed by cross-correlation with a moving average validation to obtain velocity vector maps. The size of IA was chosen as 32 × 32 pixels with an overlap of 25%.

One of the advantages of the updated DynamicStudio platform lied in its competency in performing particle characterization or "shadow processing" based on PIV images. The shadow processing function was employed in this study to acquire time-dependent position and velocity of the settling particle, which enabled simultaneous measurements of both solid and fluid phases. The positions of the illuminated settling particle in two successive images were correlated to obtain the "shadow" displacement and thus its velocity, which could be considered as instantaneous.

Two types of grains were used in this study, as summarized in Table 2. The first type of spherical grains had two diameters, 6.35 mm and 7.94 mm, and was made of polystyrene with a density of $\rho_s = 1050$ kg/m³. This grain density was calculated using the standard drag relationship (see Appendix A) and terminal velocity measured under the test conditions, and also close to the value determined by grain diameter and weight (within 1% discrepancy). In addition, for particles of the same size, the differences in mass and still water terminal velocity were found negligible. One favorable property of these polystyrene particles was their ability of scattering enough light upon laser illumination such that a whole grain appeared as a well-defined bright object under the black background (see Fig. 2). This enabled the shadow processing function to readily determine the position and thus the velocity of the settling particle.

The second type of particles, with an average density of 1077 kg/m³, was made by cutting a plastic cord into segments. These grains were approximately cylindrical in shape with an average length of 3.0 mm and diameter of 2.4 mm. Their volume-equivalent nominal diameters varied from 2.8 mm to 3.1 mm. Preliminary tests showed that the particle properties varied from grain to grain, e.g. the mass and the still water settling velocity. To avoid uncertainties induced by such variations, the still water terminal velocity, W_T, was measured individually prior to settling tests for each grain. The measured W_T ranged from 2.05 to 5.92 cm/s and the particle Reynolds number Re_p, based on the volume-equivalent nominal diameter, varied from 66 to 198.

3. Experimental results

3.1. Turbulent flow conditions

With the PIV measurements, a double-average technique was applied to generate average and RMS values of the flow velocity in both horizontal and vertical directions. The two average velocities, horizontal component U and vertical component V, are computed as follows:

$$U = \frac{1}{N}\sum_{i=1}^{N} u_i, \qquad V = \frac{1}{N}\sum_{i=1}^{N} v_i. \tag{1}$$

The corresponding RMS values are given by

$$U' = \sqrt{\frac{1}{N}\sum_{i=1}^{N}(u_i - U)^2}, \qquad V' = \sqrt{\frac{1}{N}\sum_{i=1}^{N}(v_i - V)^2}, \tag{2}$$

where N denotes the total number of the velocity vectors involved in the image processing. The N-value was computed as $n_1 \times n_2$. Here, n_1 is the number of the velocity vectors for each PIV image pair, and n_2 is the number of all image pairs captured for each run with a single particle passing through the flow zone imaged. The number of image pairs, n_2, varies from 4 to 14 in the study, corresponding to time duration of 0.364–1.273 s at the sampling rate of 11 Hz.

Two approaches were adopted in this study to quantify the flow field relevant to the settling process, with two types of observation frames, as summarized in Table 3. First, a "large" observation frame,
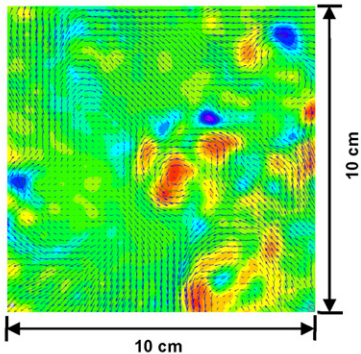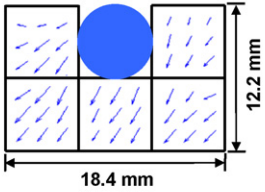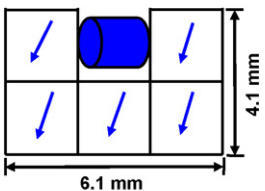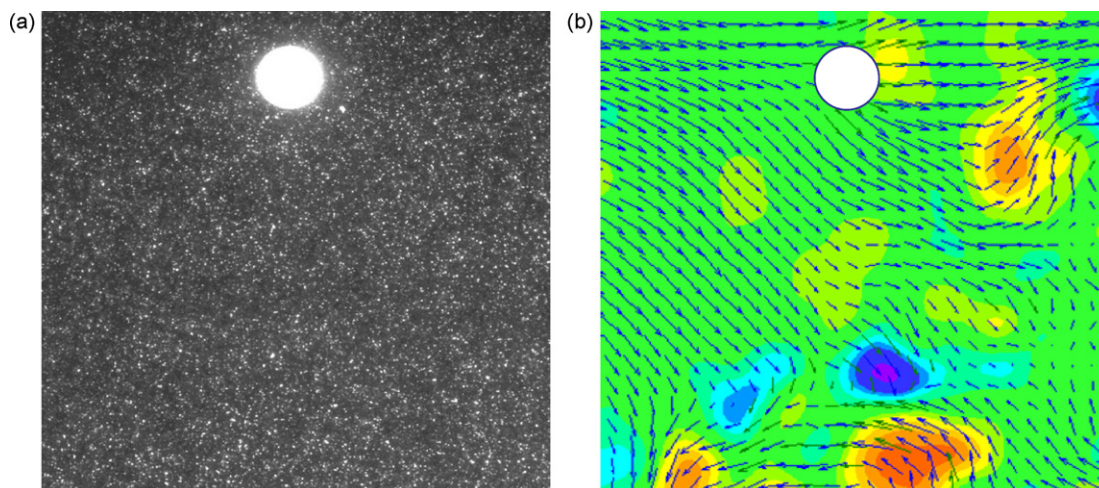

Fig. 2. (a) An example of PIV raw images, with large white spherical object being settling particle and tiny white dots being seeding particles; (b) an example of derived flow vector map.

Table 3
Definitions of observation frames.

Definitions of observation frames

Type of observation frame	Sketch with dimensions		Number of vectors n_1
Large frame - fixed - covering whole imaging window	10 cm × 10 cm		2401
Small frame - dynamic - covering local flow near settling particle	Spherical particle	18.4 mm × 12.2 mm	45
	Cylindrical particle	6.1 mm × 4.1 mm	5

fixed in position, was used to cover the whole flow section imaged. Therefore, for this approach, $n_1 = 49 \times 49 = 2401$, as detailed in the early section.

Second, we also used a "small" observation frame, which in size was comparable to the settling particle. This small frame was dynamic, covering the flow field right next to the particle in motion, as shown in Table 3. Since moving together with the settling particle, the small frame was able to acquire more specific information of the flow. It should be noted that the small frame excluded the area in the wake of the particle, as intuitively this portion of flow was already modified by the particle motion and could not provide desirable information on the background flow that directly affected the particle motion. The areas "cut off" from the whole vector map consisted of five virtual squares, two being located at the same elevation as the settling particle, and the other three being lower but immediately "in front of" the settling particle. For both sizes of the spherical particles tested, the number of vectors in each square was $3 \times 3 = 9$, and thus 5^2 added up giving that $n_1 = 45$ for each pair of images.

Altogether, 141 runs were completed for both spherical and cylindrical grains. Shown in Fig. 3 are the graphs of U and U' plotted against V and V', respectively, with both large- and small-frame processed datasets. It is observed that on average, the mean flow in the area imaged is small but generally downward. This is associated with large-scale flow structure or secondary flow inherent in the oscillating-grid system, which can be minimized but cannot be

completely removed. Experimental observations have shown that such secondary flows are usually very weak, and the relevant time scale is much longer than that of the turbulence generated. With these considerations, the secondary flows were often ignored in the previous studies (e.g. [1–3]), including the authors' early work [10]. However, the vertical component of the average velocity is considered in this study. As shown by the subsequent data analysis, the vertical velocity appears generally weak, but its effect on the settling velocity is not always minor.

In comparison to the downward bias of the vertical velocity, the horizontal component of the mean-flow, on average, is approximately zero. This can be explained by considering the orientation of the grid plane, which oscillated in the vertical direction. Being different from the mean-flow velocities, the velocity fluctuations in the vertical and horizontal directions appear positively correlated to each other, as shown in Fig. 3(c) and (d). In particular, Fig. 3(d) demonstrates that for the data collected with the small frame, the magnitude of U' is close to that of V', implying that the turbulence generated appear locally homogeneous.

3.2. Settling velocity in turbulent flow

In Fig. 4, the settling velocity observed in the presence of turbulence, W_s, is plotted against the mean vertical velocity of the flow field, V. It shows that W_s deviates significantly from the still water terminal velocity, varying from $0.4W_T$ to $1.6W_T$. However, it
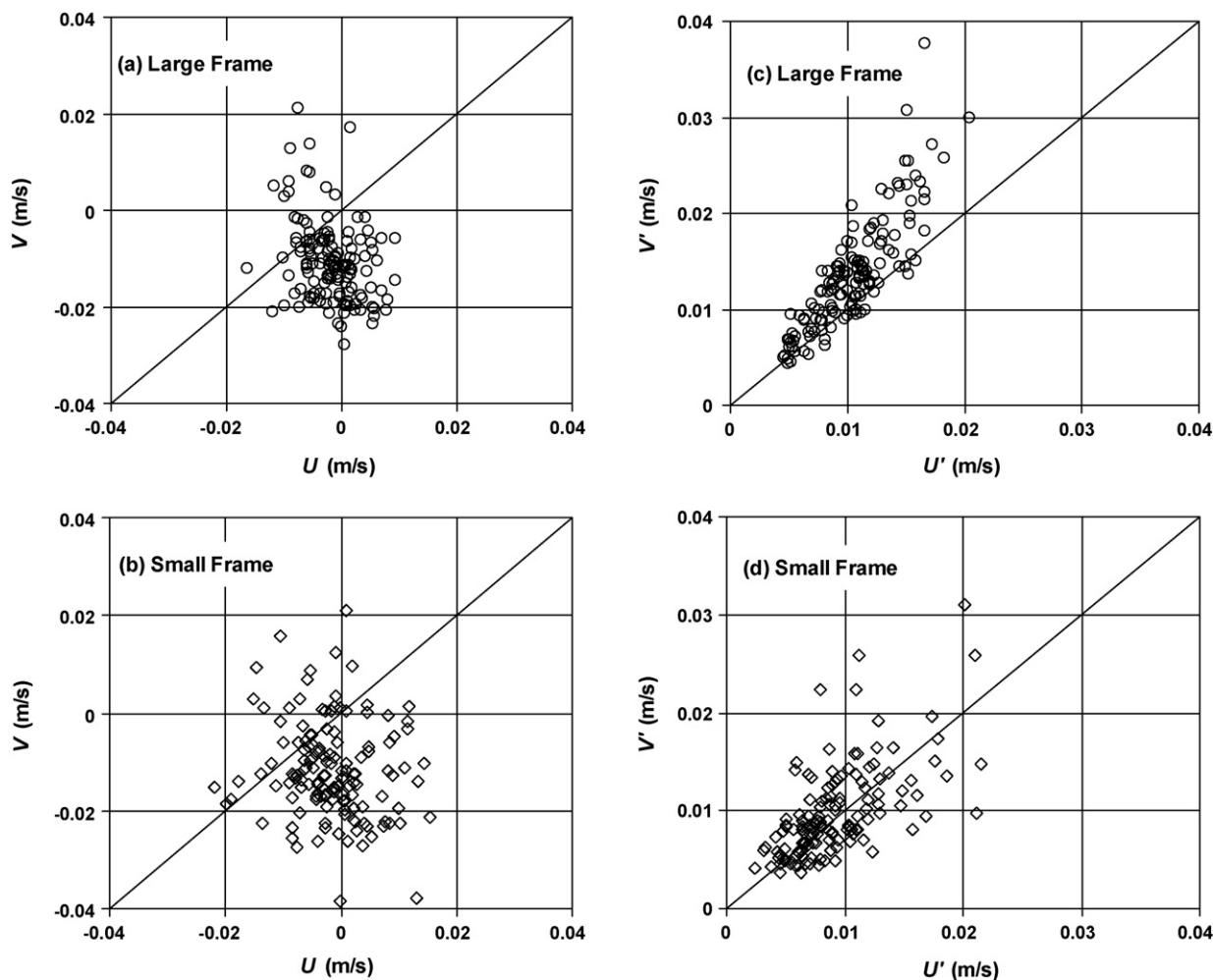
Fig. 3. Background flow conditions based on both large- and small-frame sampling: (a and b) mean vertical velocity V versus mean horizontal velocity U and (c and d) RMS vertical velocity V' versus RMS horizontal velocity U'.

can be observed that W_s has a clear correlation with V. When V is negative (i.e. downward) or V/W_T is positive, W_s/W_T is generally greater than unity, implying an enhanced settling rate, and vice versa. It should be mentioned here that by definition, the vertical upward velocity is positive, and the downward settling velocity, W_T or W_s, is taken to be negative. By comparing Fig. 4(a) and (b), it appears that the small-frame sampling yields a better correlation. This discrepancy between the two approaches should be attributed to the non-uniformity of the flow field. This result further implies the necessity to correlate the settling velocity modification only to the properties of the flow very close to the moving particle, such as the small frame used in this study.

3.3. Relative settling velocity or slip velocity

In this section, the observed settling velocity, W_s, is modified by subtracting the mean vertical velocity of the fluid, V, which yields the vertical velocity of the solid relative to the fluid phase, or the slip velocity. Only the small-frame data are used here for the analysis. As summarized in Table 4, altogether 12 cases (composed of 123 runs) for spherical particles are considered, which include two particle sizes (d), two grid oscillating frequencies (f), and three imaging zones (z).

Fig. 5 shows a histogram of the velocity ratio, $(W_s - V)/W_T$. It can be seen that the relative settling velocity ranges approximately from $0.7W_T$ to $1.1W_T$. The average of the velocity ratio is 0.92 and 0.93 for d = 6.35 mm and 7.94 mm, respectively. Both distributions peak

approximately at 0.94. Fig. 5 also shows that the relative settling velocity ($W_s - V$) is smaller than the terminal velocity for the most cases, i.e. 84% of the data for d = 6.35 mm and 92% for d = 6.35 mm.

3.4. Variations in drag coefficient

The drag coefficient C_D, as a function of Reynolds number Re, is plotted Fig. 6. Both parameters are computed based on the slip velocity, $W_s - V$. As expected, the turbulence-affected C_D deviates from the standard drag curve, the latter being computed using the correlation proposed by Cheng [20] that gives an excellent representation of experimental data (see Appendix A). Moreover, Fig. 6 also shows the inverse-square dependence of C_D on Re, as given by $C_D = (4/3)((gd^3(\rho_s/\rho - 1))/\nu^2)(1/Re^2)$ that can be derived by combining both definitions of C_D and Re. The two datasets follow different trends, which correspond to the different particle sizes. The slight scattering within each dataset is due to the changes in temperature (from 23 to 24 °C) and thus the water viscosity. The plotted C_D–Re relationship serves as an alternative to the quantification of turbulence effects on the settling velocity; however, it does not provide any information on turbulence properties and their correlations to the modification in the drag coefficient.

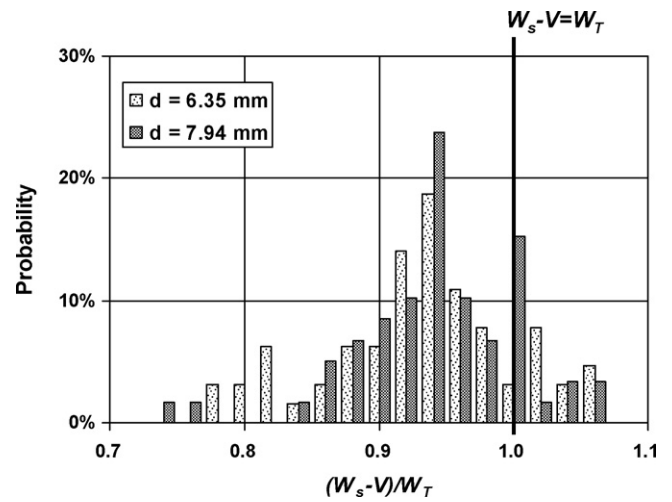### 3.5. Effects of fluid velocity fluctuations

To correlate the modification in the relative settling velocity with the turbulent flow properties, the velocity fluctuations, i.e.
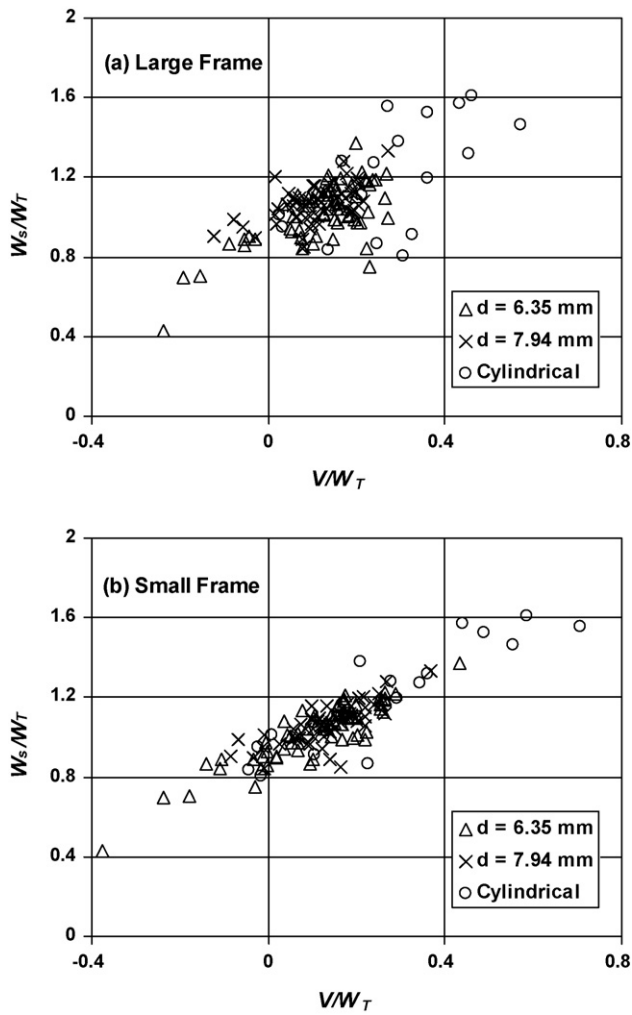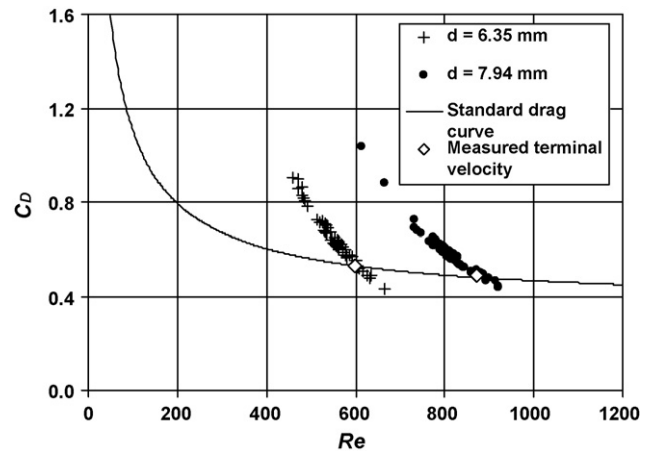
Fig. 4. Settling velocity W_s as a function of mean vertical flow velocity V, both normalized by still water terminal velocity W_T, with V calculated based on (a) large frame and (b) small frame.

Fig. 5. Histogram of relative velocity ratio $(W_s - V)/W_T$ in analysis bin of 0.02.

Fig. 6. Turbulence-affected drag coefficient C_D versus Reynolds number Re relationship (computed based on relative settling velocity $W_s - V$), in comparison to standard drag curve.

U' and V', were computed for each run to quantify the degree of turbulence.

In Fig. 7 the turbulence-modified relative settling velocity is plotted against the velocity fluctuations computed based on both large and small frames. It can be observed that the ratio, $(W_s - V)/W_T$, is generally smaller than unity, which suggests a reduction in the relative settling velocity due to turbulence. This phenomenon might be associated with the change in the location of the flow separation around the particle surface due to the ambient turbulence. Note that unstable wake may start to shed periodically

around a sphere at $Re = 150$. In this study, Re varied from 458 to 921 (see Fig. 6), and thus the vortex shedding could be the dominant factor affecting the size and shape of the wake, and thus the drag. However, Fig. 7 gives no clear trend of the relation of the fluid velocity fluctuations with the settling velocity reduction. This may be partially due to the narrow range of the physical properties (fluid and particles) covered in the present study.

As shown in Table 4, each case consists of several runs of tests for the spherical particles. If the turbulence is considered stationary for each case, Fig. 7 can be simplified by replacing the data points

Table 4
Test conditions and averaged velocity ratios for spherical particles.

| Case	d (mm)	f (Hz)	z (m)	No. of runs tested	W_s/W_T	$(W_s - V)/W_T$
1	6.35	2	0.034–0.134	14	1.106	0.955
2	6.35	2	0.091–0.191	12	1.046	0.895
3	6.35	2	0.163–0.263	10	1.098	0.974
4	6.35	3	0.034–0.134	10	1.022	0.865
5	6.35	3	0.091–0.191	8	1.032	0.924
6	6.35	3	0.163–0.263	10	0.839	0.913
7	7.94	2	0.034–0.134	8	1.122	0.926
8	7.94	2	0.091–0.191	15	1.057	0.898
9	7.94	2	0.163–0.263	10	1.041	0.935
10	7.94	3	0.034–0.134	10	1.080	0.931
11	7.94	3	0.091–0.191	6	1.115	0.940
12	7.94	3	0.163–0.263	10	1.003	0.981
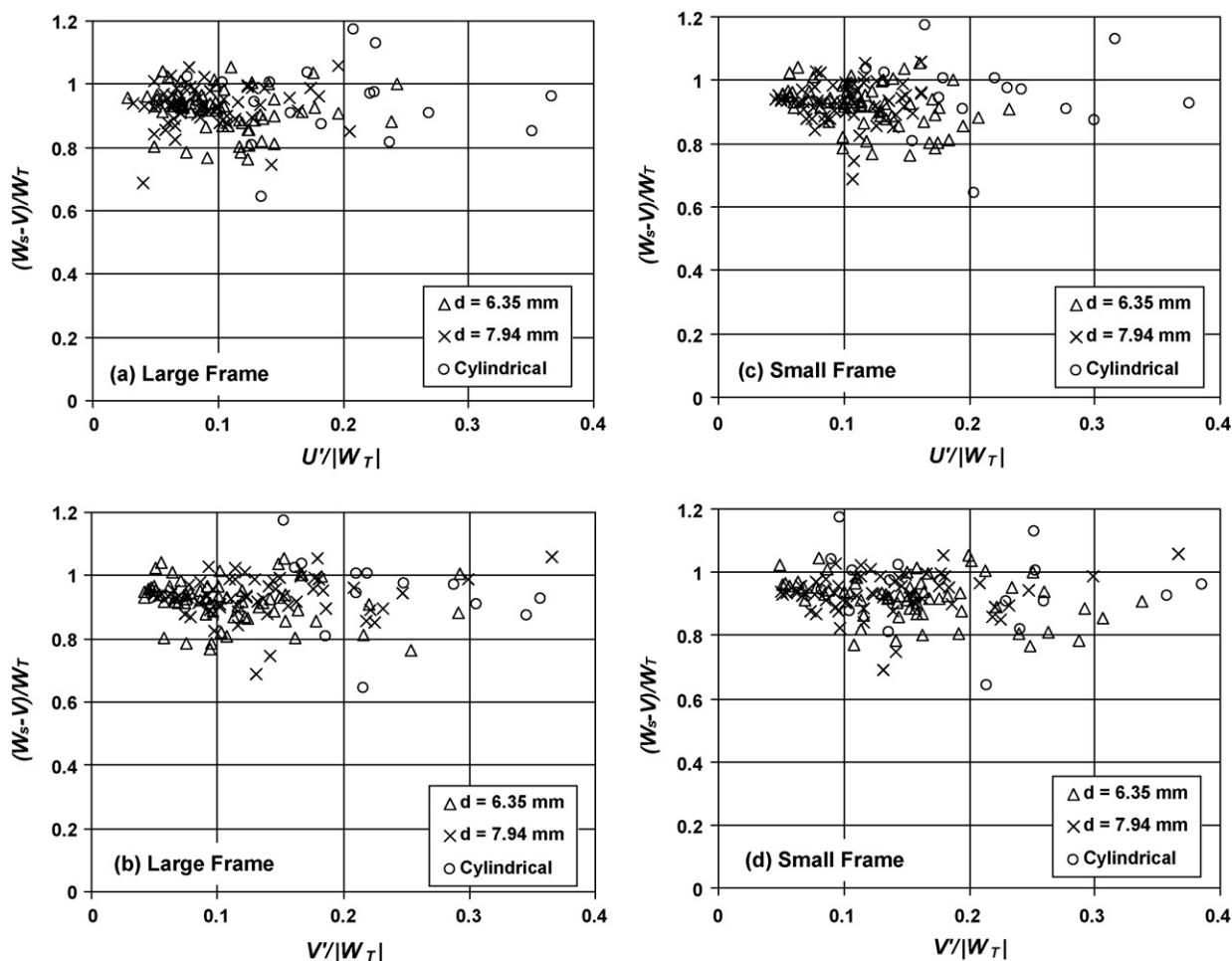
Fig. 7. Variations of relative settling velocity $W_s - V$ with horizontal and vertical flow velocity fluctuations (U' and V', respectively).

with case-averaged values. The results so obtained are then plotted in Fig. 8, which suggests that the relative settling velocity decreases slightly with increasing velocity fluctuation.

3.6. Settling velocity fluctuation

It was observed that the particle, subjected to its ambient turbulent flow, never settled at a constant rate and thus the settling velocity fluctuated along the settling course. Such fluctuations were evaluated by performing trajectory analysis for all 141 runs based on the shadow processing results, which provided position-time relationships of the settling particles at the frequency of 11 Hz. The quasi-instantaneous settling velocity was first computed from the particle displacement within the sampling interval of 1/11 s. For each run, the settling velocity fluctuation, W_s', was then computed as the standard deviation of all the quasi-instantaneous values observed. A histogram of the observed settling velocity fluctuation, W_s', normalized by the terminal velocity W_T, is shown in Fig. 9. The relevant numerical values are also tabulated in Table 5. It can be seen that W_s'/W_T varies from 2.6% to 53.6% in the presence of tur-

bulence, which is significantly larger than the fluctuation under still water (3.3–4.7%). Fig. 10 reveals that W_s' is generally comparable to the vertical velocity fluctuations of the fluid, V' (computed based on the small frame), which implies an intensive phase-to-phase interaction.

3.7. Similar observations with cylindrical grains

The analyses in Sections 3, 4 and 5 are performed largely with the data obtained for the spherical particles only. Similar results were also obtained for the cylindrical plastic particles, as summarized in Table 6. As shown in Figs. 4, 7 and 10, these results are consistent with the observations with the spherical particles, in spite of the different particle shape. It is noted that for the cylindrical particles that are smaller than the spherical particles, the size of the "small" observation frame was reduced, as shown in Table 3, and therefore n_1 was also reduced to 5, in comparison with 45 used for the spherical particles.

4. Comparison with other studies

In this section, further data analyses are made with dimensional considerations, in particular, by comparing with the similar experimental studies by Doroodchi et al. [9] and Brucato et al. [2], both reporting settling velocity reduction due to turbulence.

Doroodchi et al. [9] conducted their experiments with particle sizes comparable with those used in the present study, and turbulence generated by a pair of grids oscillating horizontally. A
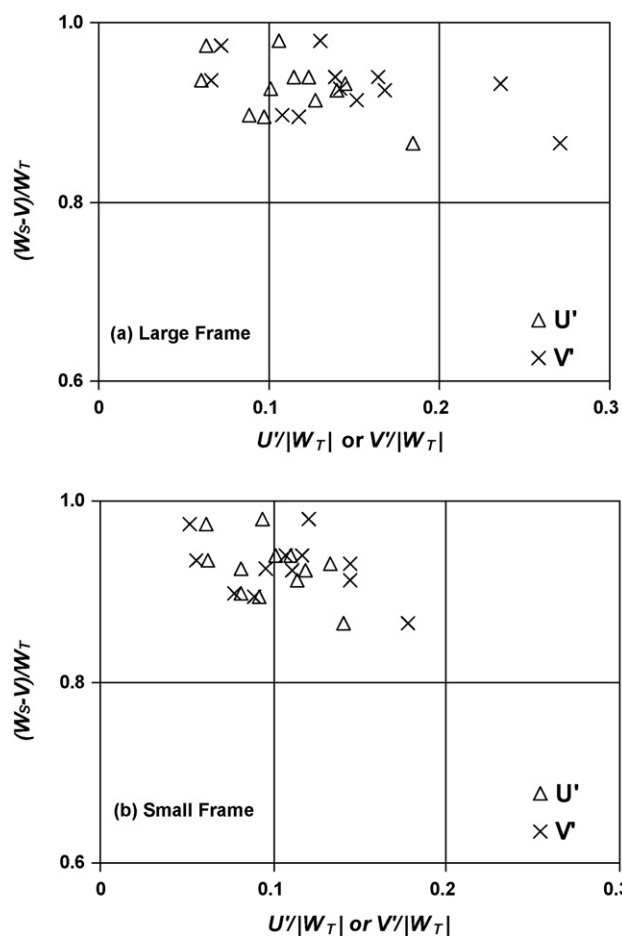
Table 5
Observed settling velocity fluctuations (in % of terminal velocity).

d (mm)	Still water condition	Turbulence-affected condition		
		Maximum	Minimum	Mean
6.35	3.34	53.6	2.66	12.6
7.94	4.73	45.0	2.63	10.8

Fig. 8. Averaged relative settling velocity, $W_s - V$, in relation to averaged horizontal and vertical flow velocity fluctuations (U' and V', respectively).

Fig. 9. Histogram of settling velocity fluctuations over terminal velocity ratio W_s'/W_T in analysis bin of 0.01.

Fig. 10. Settling velocity fluctuation W_s' as a function of vertical flow velocity fluctuation V' (small frame data), both normalized by still water terminal velocity W_T.

high-speed camera was used to record the settling processes and the settling velocity was computed from particle trajectory, which is similar to the present study. However, no direct measurements were performed on the fluid phase in their study. The flow characteristics of the turbulence were assumed to be identical to similar measurements by Yang and Shy [11].

To compare with Doroodchi et al.'s results [9], it is necessary to have several quantities defined for the present study. First, the
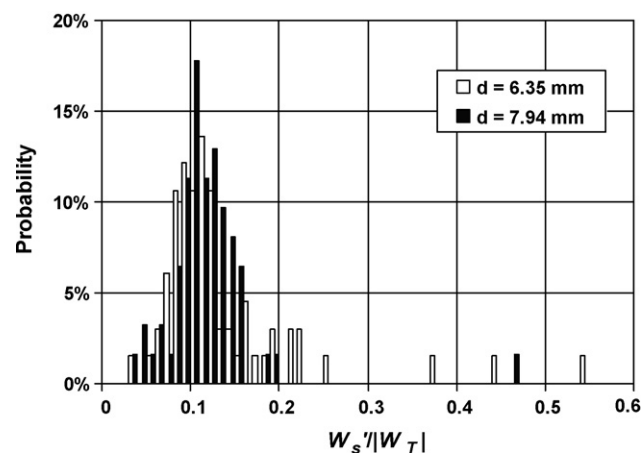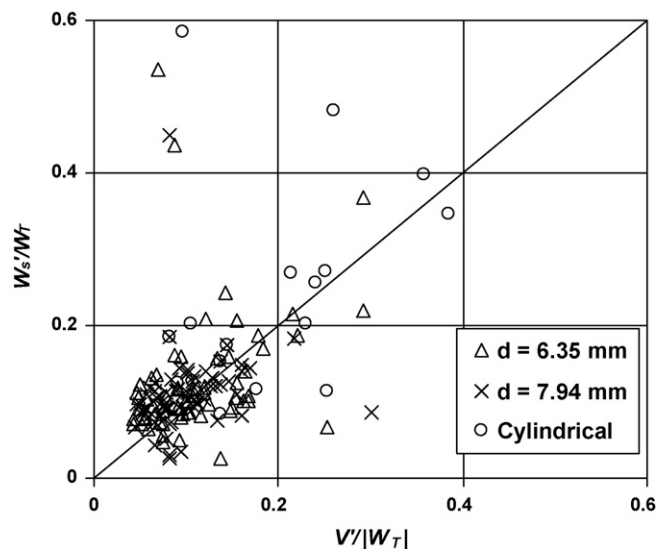
Table 6
Test conditions and settling velocity ratios for cylindrical particles.

Case	d_* (mm)	Re_p	f (Hz)	z (m)	W_s/W_T	$(W_s - V)/W_T$	W_s'/W_T
1	2.779	122	2	0.116–0.216	1.282	1.005	0.126
2	2.945	134	2	0.073–0.173	1.607	1.022	0.174
3	2.846	161	2	0.073–0.173	0.950	0.974	0.152
4	3.037	182	2	0.073–0.173	1.112	0.945	0.186
5	2.763	66	2	0.073–0.173	1.321	0.962	0.345
6	3.037	153	2	0.073–0.173	1.075	0.972	0.116
7	2.903	98	2	0.073–0.173	1.464	0.909	0.481
8	2.998	110	2	0.073–0.173	1.199	0.907	0.203
9	2.882	178	2	0.073–0.173	1.015	1.006	0.114
10	3.031	198	2	0.073–0.173	1.381	1.172	0.584
11	3.112	179	2	0.073–0.173	0.869	0.643	0.269
12	2.817	132	2	0.073–0.173	0.832	0.875	0.203
13	2.978	114	2	0.073–0.173	1.571	1.131	0.271
14	2.985	67	2	0.073–0.173	0.803	0.818	0.255
15	2.985	67	2	0.073–0.173	1.559	0.852	0.497
16	2.952	137	2	0.073–0.173	1.269	0.927	0.398
17	3.050	188	2	0.073–0.173	0.916	0.809	0.083
18	2.972	176	2	0.073–0.173	1.526	1.039	0.124

Note: d_* is volume-equivalent nominal diameter for cylindrical particles; and particle Reynolds number Re_p is calculated based on still water terminal velocity.
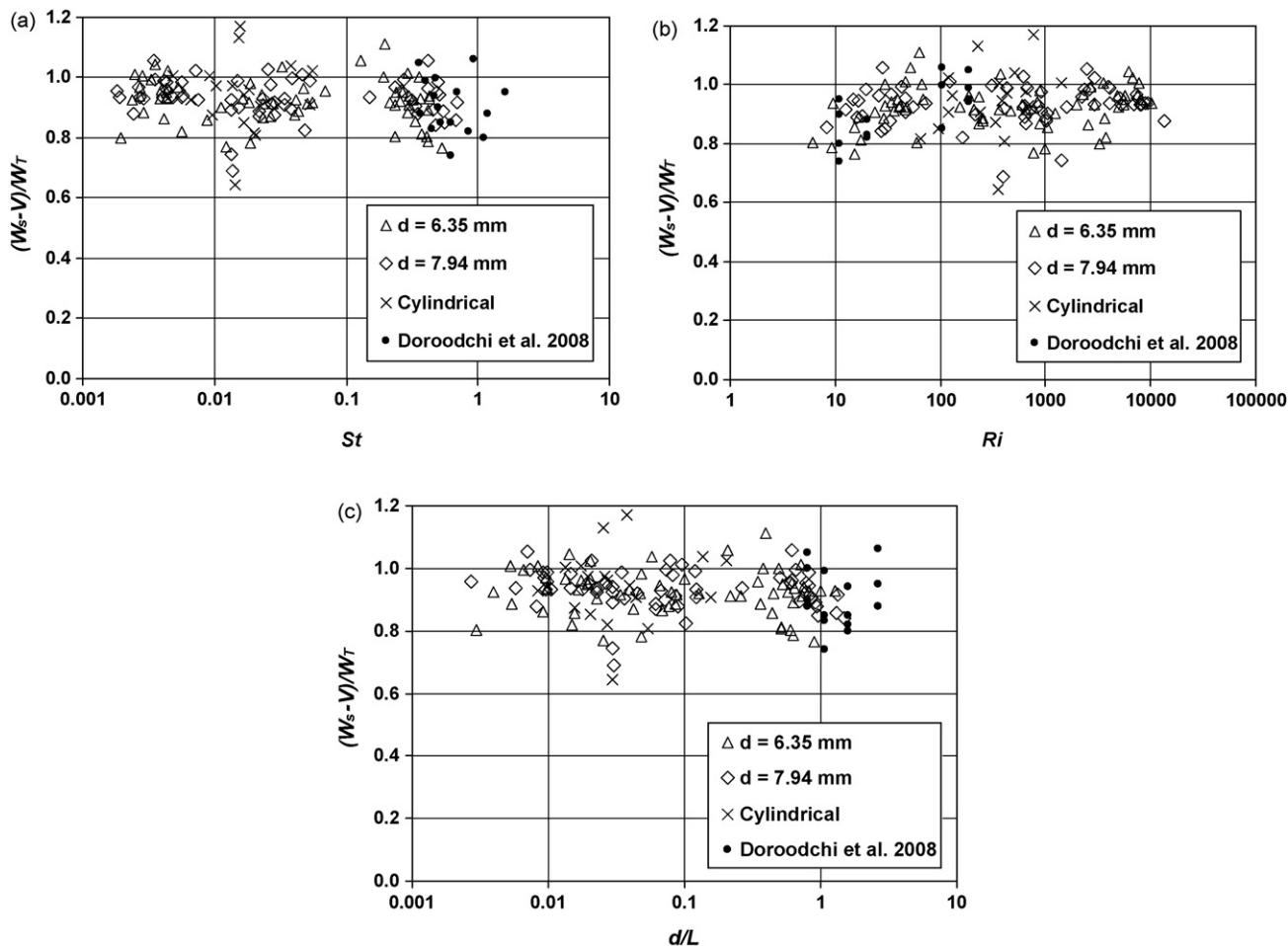
Fig. 11. Variation of relative settling velocity ratio, $(W_s - V)/W_T$, with (a) St, (b) Ri, and (c) d/L, in comparison to data by Doroodchi et al. [9].

energy dissipation rate, ε, is estimated using the analytical solution for the turbulent flow proposed by Matsunaga et al. [18], as detailed in Appendix B. Then, the integral length scale of turbulence is given by $L = U'^3/\varepsilon$, where U' is the measured horizontal velocity fluctuation. Also, following Doroodchi et al. [9], the particle relaxation time, which characterizes the time scale of particle–fluid interaction, is expressed as $\tau_p = (\rho_s/(\rho + C_A))/((3/4)(C_{D0}/d)W_T)$, where C_{D0} is the standard drag coefficient and $C_A = 0.5$ is the added mass coefficient. It should be noted that a time scale so defined might be more suitable for large-sized particles in the present study, as compared to the Stokes response time, $t_p = W_T/g = \rho_s d^2/18\rho\nu$, which was commonly adopted by some other researchers, e.g. Cuthbertson and Ervine [4] and Kawanisi and Shiozaki [5], for small-sized particles moving in or near the Stokes range. In addition, the integral time scale of turbulence, T_L, is expressed as $T_L = L/U'$. The Stoke number, St, representing the particle-over-turbulence time scale ratio, is then defined as $St = \tau_p/T_L = \tau_p U'/L$. One more dimensionless number, the Richardson number is defined as $Ri = (g|\rho_p - \rho|/\rho)(L/U'^2)$, which represents the ratio of the net effective weight of the particle due to gravity to the inertial force due to turbulence [9].

Fig. 11 shows the variation in the velocity ratio, $(W_s - V)/W_T$, observed in the present study with the three dimensionless parameters, St, Ri and d/L, respectively. Also plotted in the figure are the data points reported by Doroodchi et al. [9]. From Fig. 11, it follows that the reductions in the relative settling velocity observed in this study are comparable to those reported by Doroodchi et al. [9]. However, with the three parameters varying in much wider ranges for this study, no clear trend can be observed in the dependence of

$(W_s - V)/W_T$ on St, Ri or d/L. This result could indicate that none of the three parameters considered is dominant for the particle-flow interaction considered here.

Brucato et al. [2] reported reduction in the settling velocity of solid particles in a stirred medium with respect to that in a quiescent liquid. They measured the mean settling velocity of a cloud of glass and silica particles using a residence time technique in the turbulent flow generated in a Couette–Taylor stirred vessel. They proposed a correlation between W_s/W_T and the length scale ratio d/λ, where d denotes the particle diameter and λ the Kolmogorov scale of dissipative eddies defined as $\lambda = (\nu^3/\varepsilon)^{1/4}$. Brucato et al. [2] further related the turbulence affected drag coefficient C_D to the length scale ratio d/λ in the form of $(C_D - C_{D0})/C_{D0} = 8.76 \times 10^{-4}(d/\lambda)^3$, where C_{D0} denoted the standard drag coefficient. In Fig. 12, the present data are compared with Brucato et al.'s relation. The large difference suggests that the relation based on the Kolmogorov scale is not applicable for the present study. This is probably due to the much higher density and smaller sizes of the particles used in Brucato et al.'s tests (see Table 1), as compared to the present study. In addition, a much smaller reduction in the settling velocity (up to 30% of W_T) is observed in the present study, as compared to 85%, a maximum reported by Brucato et al. [2].

5. Estimate of turbulence-modified settling velocity

With the limited knowledge of particle–turbulence interaction, to exactly predict turbulence-modified settling velocity is almost
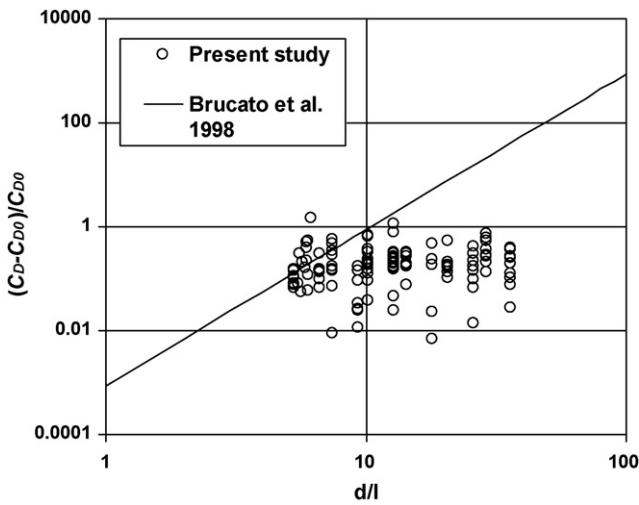
Fig. 12. Variations of normalized drag coefficient $(C_D - C_{D0})/C_{D0}$ with length scale ratio d/λ, with comparison to correlation proposed by Brucato et al. [2] (*Note*: negative values for $(C_D - C_{D0})/C_{D0}$ are not displayed).

impossible at present. In the following, a simple model is proposed to estimate the changes in the settling velocity for the condition considered in this study.

For the case of the turbulent velocity much smaller than the terminal velocity, the local velocity of a settling particle can be approximated as $(|W_T| - v)$, where v is the local velocity of the fluid. Following Davila and Hunt [21], the time for a particle traveling a vertical distance ΔL, which is much longer than turbulence integral scale, is then given by

$$\Delta t = \frac{1}{|W_T|} \int_0^{\Delta L} \frac{dz}{1 - v/|W_T|}. \tag{3}$$

In the case of $|v| \ll |W_T|$, applying series expansion to the above equation yields:

$$\Delta t = \frac{1}{|W_T|} \int_0^{\Delta L} \left[1 + \frac{v}{|W_T|} + \left(\frac{v}{|W_T|}\right)^2 + \left(\frac{v}{|W_T|}\right)^3 + \cdots \right] dz. \tag{4}$$

By defining the average settling velocity as $\Delta L/\Delta t$, then

$$\frac{1}{|W_s|} = \frac{1}{|W_T|} \left(1 + \frac{\langle v \rangle}{|W_T|} + \frac{\langle v^2 \rangle}{|W_T^2|} + \frac{\langle v^3 \rangle}{|W_T^3|} + \cdots \right), \tag{5}$$

where $\langle \rangle$ denotes average values. Furthermore, by taking $\langle v \rangle = V$ and $\langle v^2 \rangle = V^2 + V'^2$, and ignoring the terms with the third and higher orders, we get

$$|W_s| = \frac{|W_T|}{1 + V/|W_T| + V^2 + V'^2/|W_T^2|}. \tag{6}$$

Eq. (6) indicates that the settling velocity is modified by both mean vertical velocity and turbulence intensity, and if the secondary flow is negligible and thus $V = 0$, the reduction in the settling velocity, $(|W_T| - |W_s|)/|W_T|$, is approximately proportional to $(V'/W_T)^2$. The computed settling velocities using Eq. (6) for both small and large frames are plotted in Fig. 13, in comparison with the measurements. It shows that the agreement is reasonably good, in particular for the data collected with the small frame. The average of the relative error, defined as $|(W_{s\,predicted} - W_{s\,measured})/W_{s\,measured}|$, is 9.4% and 8.3% for the case of large- and small-frame, respectively.
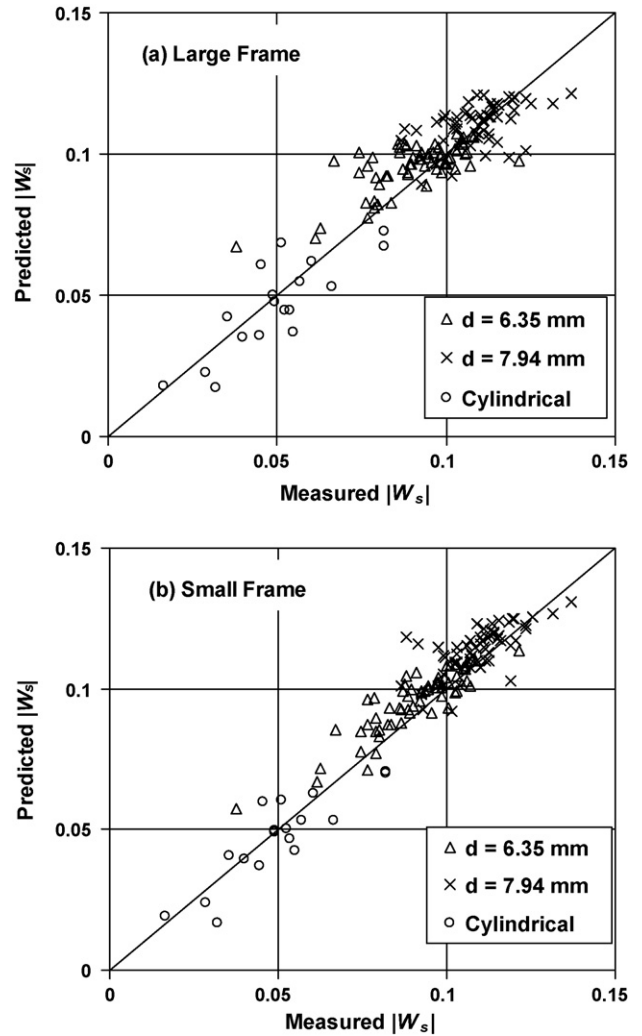
Fig. 13. Comparison of settling velocity predicted by Eq. (6) and measurements, with flow sampling based on (a) large frame and (b) small frame.

6. Conclusions

In this study, the settling behavior of various types of particles, which were a few millimeters in size and slightly heavier than water, was investigated in the turbulent field generated by an oscillating grid. Flow information of both solid and fluid phases was sampled simultaneously with digital PIV, together with its enhanced shadow processing function.

The relative settling velocity was observed to be generally smaller than the still water terminal velocity. However, the reduced settling velocity cannot be simply correlated to turbulence intensity or other dimensionless parameters including the Stokes number. On the other hand, the experimental results also show that the fluctuation in the settling velocity is significant as compared to the still water case, and also correlates with the vertical velocity fluctuation of the turbulence, implying intensive inter-phase interactions. To estimate the turbulence-modified settling velocity, a simple analytical model was finally proposed in this study, which shows that the reduction in the settling velocity, if the vertical mean flow is negligible, is approximately proportional to the squared RMS vertical velocity.

It should be noted that for the two-phase system employed in this study, the physical properties including particle sizes and turbulence intensities varied in the limited range, which does not allow a systematic and overall description of the phenomena and the

underlying physics. Also, only one-way analyses were performed by assuming that the particle motion does not significantly affect turbulence properties for the case of single particle settling. Further experimental efforts are needed especially with smaller-sized particles.

Appendix A. Standard drag coefficient

The standard drag coefficient, C_{D0}, can be computed by the following correlation that is applicable for the entire subcritical region (e.g., $Re < 2 \times 10^5$) [20]:

$$C_{D0} = \frac{24}{Re_p}(1 + 0.27\,Re_p)^{0.43} + 0.47[1 - \exp(-0.04\,Re_p^{0.38})]. \quad (7)$$

By comparing with other six empirical formulas, Cheng [20] shows that Eq. (7) gives the best representation of experimental data with the prediction errors less than 2.5%. Here, the standard drag coefficient C_{D0} is expressed as

$$C_{D0} = \frac{4}{3}gd\frac{\rho_s - \rho}{\rho}\frac{1}{W_T^2}, \quad (8)$$

in which g is the gravitational acceleration, d is the particle diameter, ρ_s is the solid particle density and ρ is the fluid density. Also, the particle Reynolds number Re_p is defined as

$$Re_p = \frac{|W_T|d}{\nu}, \quad (9)$$

where ν is the kinematic fluid viscosity.

Appendix B. Computation of turbulent energy dissipation rate

Following Matsunaga et al. [18], the turbulent energy k, energy dissipation rate ε, and vertical distance from the grid mid-plane z are normalized, respectively, as follows:

$$\hat{k} = \frac{k}{k_0}, \qquad \hat{\varepsilon} = \frac{\varepsilon}{\varepsilon_0}, \qquad \hat{z} = \frac{z}{(k_0^3\varepsilon_0^{-2})^{1/2}}, \quad (10)$$

where k_0 and ε_0 are introduced as the boundary conditions at $z = 0$, of which the values are estimated by the empirical expressions:

$$\frac{k_0}{f^2S^2} = 6.0 \times 10^{-1}\left(\frac{S}{M}\right)^{1/4}, \quad (11)$$

$$\frac{\varepsilon_0}{f^3S^2} = 4.5 \times 10^{-1}\left(\frac{S}{M}\right) \quad (12)$$

for $fS^2/\nu \geq 5500$. Both $\hat{k}$ and $\hat{\varepsilon}$ are related to $\hat{z}$ in the power form:

$$\hat{k} = \left(\frac{\hat{z}}{1.82} + 1\right)^{-5}, \quad (13)$$

$$\hat{\varepsilon} = \left(\frac{\hat{z}}{1.82} + 1\right)^{-8.5}. \quad (14)$$

In the present study, a spatial averaging of k and ε is done by integrating over the respective z ranges covered by the imaging windows (summarized in Tables 4 and 6), as expressed by the following equations:

$$k_{mean} = \hat{k}_{mean}k_0 = \frac{\int_{\hat{z}=\hat{z}_{lower}}^{\hat{z}_{upper}}[(\hat{z}/1.82 + 1)^{-5}]\,d\hat{z}}{\int_{\hat{z}=\hat{z}_{lower}}^{\hat{z}_{upper}}d\hat{z}}k_0$$

$$= \frac{[1.82/ - 4(\hat{z}/1.82 + 1)^{-4}]_{\hat{z}_{lower}}^{\hat{z}_{upper}}}{\hat{z}_{upper} - \hat{z}_{lower}}k_0, \quad (15)$$

$$\varepsilon_{mean} = \hat{\varepsilon}_{mean}\varepsilon_0 = \frac{\int_{\hat{z}=\hat{z}_{lower}}^{\hat{z}_{upper}}[(\hat{z}/1.82 + 1)^{-8.5}]\,d\hat{z}}{\int_{\hat{z}=\hat{z}_{lower}}^{\hat{z}_{upper}}d\hat{z}}\varepsilon_0$$

$$= \frac{[1.82/ - 7.5(\hat{z}/1.82 + 1)^{-7.5}]_{\hat{z}_{lower}}^{\hat{z}_{upper}}}{\hat{z}_{upper} - \hat{z}_{lower}}\varepsilon_0, \quad (16)$$

where $\hat{z}_{lower}$ and $\hat{z}_{upper}$ corresponds to the dimensionless vertical distance of the lower and upper boundaries of the imaging windows, respectively. Thus, k and ε can be computed to characterize the diffusion and dissipation of turbulent energy in the respective experimental conditions. A general comparability is observed between the computed k values based on the solution proposed above and the PIV measurements. The predicted k values based on Eq. (15) ranges from 1.46×10^{-5} to $7.80 \times 10^{-4}\,m^2/s^2$, while the experimental values ranges from 3.31×10^{-5} to $9.85 \times 10^{-4}\,m^2/s^2$. The latter is given by $k = (2U'^2 + V'^2)/2$ where U' and V' denote the RMS horizontal and vertical velocity fluctuations, respectively, based on the large observation frame. This observation, to a certain extent, justifies the applicability of the solution proposed by Matsunaga et al. [18] in the present study.

References

[1] F. Magelli, D. Fajner, M. Nocentini, G. Pasquali, Solid distribution in vessels stirred with multiple impellers, Chem. Eng. Sci. 45 (3) (1990) 615–625.
[2] A. Brucato, F. Grisafi, G. Montante, Particle drag coefficients in turbulent fluids, Chem. Eng. Sci. 53 (18) (1998) 3295–3314.
[3] J. Ruiz, D. Macias, F. Peters, Turbulence increases the average settling velocity of phytoplankton cells, PNAS 101 (51) (2004) 17720–17724.
[4] A.J.S. Cuthbertson, D.A. Ervine, Experimental study of fine sand particle settling in turbulent open channel flows over rough porous beds, J. Hydraul. Eng. 133 (8) (2007) 905–916.
[5] K. Kawanisi, R. Shiozaki, Turbulent effects on the settling velocity of suspended sediment, J. Hydraul. Eng. 134 (2) (2008) 261–266.
[6] C.Y. Yang, U. Lei, The role of the turbulent scales in the settling velocity of heavy particles in homogeneous isotropic turbulence, J. Fluid Mech. 371 (1998) 179–205.
[7] A. Aliseda, A. Cartellier, F. Hainaux, J.C. Lasheras, Effect of preferential concentration on the settling velocity of heavy particles in homogeneous isotropic turbulence, J. Fluid Mech. 468 (2002) 77–105.
[8] P.D. Friedman, J. Katz, Mean rise rate of droplets in isotropic turbulence, Phys. Fluids 14 (9) (2002) 3059–3073.
[9] E. Doroodchi, G.M. Evans, M.P. Schwarz, G.L. Lane, N. Shah, A. Nguyen, Influence of turbulence intensity on particle drag coefficients, Chem. Eng. J. 135 (1–2) (2008) 129–134.
[10] Q. Zhou, N.S. Cheng, Particle settling behavior in turbulent flow generated by oscillating grid, in: F.G. Zhuang, J.C. Li (Eds.), New Trends in Fluid Mechanics Research—Proceedings of the Fifth International Conference on Fluid Mechanics, 2007, pp. p142–145.
[11] T.S. Yang, S.S. Shy, The settling velocity of heavy particles in an aqueous near-isotropic turbulence, Phys. Fluids 15 (4) (2003) 868–880.
[12] L.P. Wang, M.R. Maxey, Settling velocity and concentration distribution of heavy-particles in homogeneous isotropic turbulence, J. Fluid Mech. 256 (1993) 27–68.
[13] R. Mei, Effect of turbulence on the particle settling velocity in the nonlinear drag range, Int. J. Multiphase Flow 20 (2) (1994) 273–284.
[14] P. Nielsen, Coastal Bottom Boundary Layers and Sediment Transport, World Scientific, 1992.
[15] P. Bagchi, S. Balachandar, Effect of turbulence on the drag and lift of a particle, Phys. Fluids 15 (11) (2003) 3496–3513.
[16] N.S. Cheng, A.W.K. Law, Measurements of turbulence generated by oscillating grid, J. Hydraul. Eng. 127 (3) (2001) 201–208.
[17] E.J. Hopfinger, T.A. Toly, Spatially decaying turbulence and its relation to mixing across density interfaces, J. Fluid Mech. Part 1 (1976) 155–175.
[18] N. Matsunaga, Y. Sugihara, T. Komatsu, A. Masuda, Quantitative properties of oscillating-grid turbulence in a homogeneous fluid, Fluid Dyn. Res. 25 (3) (1999) 147–165.
[19] J. Yan, N.S. Cheng, H.W. Tang, S.K. Tan, Oscillating-grid turbulence and its applications: a review, J. Hydraul. Res. 45 (1) (2007) 26–32.
[20] N.S. Cheng, Comparison of formulas for drag coefficient and settling velocity of spherical particles, Powder Technol. 189 (3) (2009) 395–398.
[21] J. Davila, J.C.R. Hunt, Settling of small particles near vortices and in turbulence, J. Fluid Mech. 440 (2001) 117–145.